ACS APPLIED MATERIALS & INTERFACES

Research Article

www.acsami.org

Hierarchically Oriented Macroporous Anode-Supported Solid Oxide Fuel Cell with Thin Ceria Electrolyte Film

Yu Chen,[†] Yanxiang Zhang,[†,‡] Jeffrey Baker,[†] Prasun Majumdar,[†] Zhibin Yang,[§] Minfang Han,*[,§] and Fanglin Chen*[,†]

[†]Department of Mechanical Engineering , University of South Carolina, Columbia, South Carolina 29205, United States

[‡]School of Materials Science and Engineering, Harbin Institute of Technology, Harbin 150001, People's Republic of China

[§]School of Chemical & Environment Engineering, China University of Mining & Technology, Beijing 100083, People's Republic of China

ABSTRACT: Application of anode-supported solid oxide fuel cell (SOFC) with ceria based electrolyte has often been limited by high cost of electrolyte film fabrication and high electrode polarization. In this study, dense $Gd_{0.1}Ce_{0.9}O_2$ (GDC) thin film electrolytes have been fabricated on hierarchically oriented macroporous NiO−GDC anodes by a combination of freeze-drying tape-casting of the NiO−GDC anode, drop-coating GDC slurry on NiO−GDC anode, and co-firing the electrolyte/anode bilayers. Using 3D X-ray microscopy and subsequent analysis, it has been determined that the NiO−GDC anode substrates have a porosity of around 42% and channel size from around 10 μm at the electrolyte side to around 20 μm at the other side of the NiO−GDC (away from the electrolyte), indicating a hierarchically oriented macroporous NiO−GDC microstructure. Such NiO−GDC microstructure shows a tortuosity factor of ∼1.3 along the thickness direction, expecting to facilitate gas diffusion in the anode during fuel cell operation. SOFCs with such Ni−GDC anode, GDC film (30 μm) electrolyte, and $La_{0.6}Sr_{0.4}Co_{0.2}Fe_{0.8}O_3$−GDC (LSCF−GDC) cathode show significantly enhanced cell power output of 1.021 W cm^{-2} at 600 °C using H_2 as fuel and ambient air as oxidant. Electrochemical Impedance Spectroscopy (EIS) analysis indicates a decrease in both activation and concentration polarizations. This study has demonstrated that freeze-drying tape-casting is a very promising approach to fabricate hierarchically oriented porous substrate for SOFC and other applications.

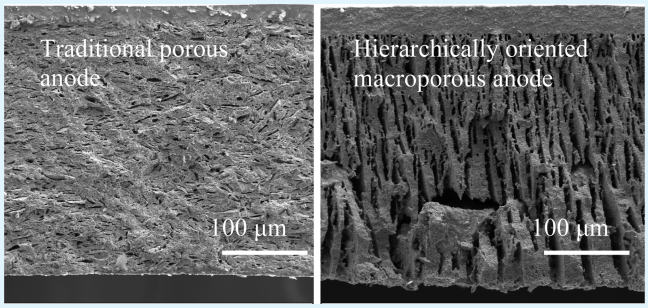

KEYWORDS: *Freeze-drying tape-casting, hierarchically oriented macropores, anode-supported solid oxide fuel cell, thin ceria electrolyte film*

1. INTRODUCTION

Solid oxide fuel cells (SOFCs) have attracted great attention as one of the most promising next generation energy conversion systems for stationary and portable applications due to the unique merits of high efficiency, low emissions and fuel flexibility.[1] Yttria stabilized zirconia (YSZ) electrolyte has been extensively used by most SOFC developers due to its superior chemical stability and almost pure oxygen-ionic conductivity over a wide range of temperature and oxygen partial pressure. Unfortunately, the ionic conductivity of YSZ becomes relatively low when the operating temperature is reduced, resulting in a substantial increase in the ohmic resistance from the electrolyte.[2] In addition, lowering the cell operating temperature will lead to a rapid increase in the interfacial polarization resistance from the electrodes.[3] However, reducing the operating temperature of SOFCs to the intermediate temperature range of 500−600 °C is beneficial to significantly lower the cost and improve the reliability of the SOFC system. Therefore, it is critical to develop highly conductive electrolyte materials as well as optimize the electrode microstructure so that the performance in both the electrolytes and electrodes can be enhanced.

Gd-doped ceria (GDC) is a promising electrolyte best suited for intermediate temperature (500−600 °C) SOFCs due to its much higher ionic conductivity compared to that of YSZ as well as chemical compatility with the state-of-the-art electrode materials. One challenge to fabricate ceria thin film electrolyte in SOFCs is the densification problem. The stringent powder fabrication process limits a broad application of dense ceria film electrolyte in SOFCs. Most of the ceria powders used in those thin film preparations were nanosized, made through hydrothermal,[4] solution combustion,[5] or co-precipitation.[6] The densification of thin electrolyte layer deposited on anode substrate can be greatly influenced by the shrinkage of the anode substrate.[7] In this work, a simple and cost-effective co-firing process has been applied in fabrication of dense GDC

Received: January 17, 2014
Accepted: March 12, 2014
Published: March 12, 2014

   dx.doi.org/10.1021/am5003662 | ACS Appl. Mater. Interfaces 2014, 6, 5130−5136

film deposited on freeze-drying tape-casted anodes using cost effective commercial GDC powders.

The traditional sponge-like porous anode substrates have been investigated extensively and proven to be benificial for the densification of electrolyte or interconnector film by drop-coating.[8−10] However, such morphology is not ideal for gas diffusion because of the high tortuosity factor, consequently limiting SOFC cell perofrmance. Although the pore structure can be modified by changing the morphology or packing of the pore formers,[11] the tortuous microstructure of the electrode still limits the cell performance.[12] Recently, a freeze-drying tape-casting method has been developed as a novel technique to form hierarchically oriented channels/pores in the SOFC electrodes.[13−15] Further, the substrates prepared by freeze-drying tape-casting in this study have the following unique features:[15,16] (i) the green tapes have adequate mechanical strength to handle for the subsequent drop-coating without the need of presintering due to the existence of organic additives; (ii) the shrinkage of the anode substrate is much higher upon sintering the green tape instead of the pre-sintered one, providing more compressive driving force to facilitate densification of ceria film; (iii) the surface of the green tapes are porous after the freeze-drying step, making a good interlocking interface between the anode and the electrolyte during the drop-coating and co-firing process. All these merits make the fabrication of dense GDC thin film electrolyte on freeze-drying tape-casted substrates possible.

In this study, freeze-drying tape-casting and co-firing have been combined to fabricate anode-supported SOFCs with hierarchically oriented macroporous anode and dense GDC thin film electrolyte. The application of these cost-effective fabrication techniques has great potential to dramatically reduce the cost of SOFC fabrication, offering a simple and economic solution for development of high performance intermediate temperature SOFCs.

2. EXPERIMENTAL STUDY

2.1. Fabrication of Anode Substrates and Cells. NiO (Sigma-Aldrich, USA), $La_{0.6}Sr_{0.4}Co_{0.2}Fe_{0.8}O_3$ (LSCF) and $Gd_{0.1}Ce_{0.9}O_2$ (GDC) powders (both from Fuel Cell Materials, USA) were purchased for this study. A NiO−GDC (mass ratio of 60:40) anode substrate was prepared by a freeze-drying tape-casting process as reported in our previous study.[15,17] The GDC electrolyte slurry was directly deposited on the green NiO−GDC anode substrates by a drop-coating process. The electrolyte/anode bi-layer was then sintered at 1400, 1450, and 1500 °C for 12 h at a heating rate of 1 °C min^{-1} before 600 °C and then at 2 °C min^{-1} after 600 °C. LSCF−GDC (mass ratio of 1:1) cathode with an active area of 0.33 cm^2 was prepared on the GDC electrolyte surface by screen-printing and then fired at 1050 °C for 2 h. For comparison, NiO−GDC anode substrate with 20 wt % graphite was prepared by dry-pressing.[8] Anode supported cells using the anode by dry-pressing with the cell configuration of NiO−GDC|GDC|LSCF−GDC have also been fabricated and evaluated. The preparation methods for electrolyte and cathode are kept the same.

2.2. Characterization. The surface of the GDC electrolyte film, anode substrate and cross-sectional view of the single cells were characterized using both scanning electron microscopy (SEM) (FEI Quanta 200) and 3D X-ray microscopy. The unique feature of three-dimensional (3D) X-ray microscopy is that it is nondestructive (as opposed to destructive techniques such as SEM/FIB-SEM) and hence allows following of a specimen before and after any changes (such as reduction or loading). In-house Matlab code was developed to calculate porosity along the thickness direction and the tortuosity factor of the NiO−GDC anode substrate fabricated from the freeze-drying tape-casting process.[18] Hydrogen (with 3 vol % H_2O) was used as a fuel while ambient air was used as an oxidant. The hydrogen flow rate was controlled at 40 sccm using a mass flow controller (APEX, Alicat Scientific). The current density-voltage curves as well as electrochemical impedance spectra (EIS) of the single cells were measured with a four probe method using a multichannel Versa STAT (Princeton Applied Research) at the operating temperature from 500 °C to 600 °C. The electrochemical impedance spectra of cells were measured under open circuit voltage over a frequency range of 1 MHz to 0.01 Hz. The ohmic resistance (R_Ω) was determined from the high frequency intercept of the impedance spectra with the real axis while the cell interfacial polarization resistance (R_p) was determined from the difference between the low and high frequency intercepts of the impedance spectra with the real axis in the Nyquist plot.

3. RESULTS AND DISCUSSION

During solidification of aqueous NiO−GDC slurry, formation of ice from water rejects not only organic additives but also inorganic ceramic powders.[19] Subsequent removal of ice crystals by sublimation during the freeze-drying process results in the formation of pores. The substrates obtained from freeze-drying tape-casting always show a graded porous structure due to the exaggerated growth of ice crystal.[16,20] In the freeze tape-casting, ice crystals first nucleated on the surface of chilling polymer film (−70 °C in this study) and then grew upwards through the temperature gradient, causing the crystals to diverge, forming continuous graded pores/channels, in which some of them spanned the entire thickness of the substrate, resulting in a less tortuous structure. Microscopic images in Figure 1 display the morphology of NiO−GDC substrate made through freeze-drying tape-casting after sintered at 1450 °C for 12 h.

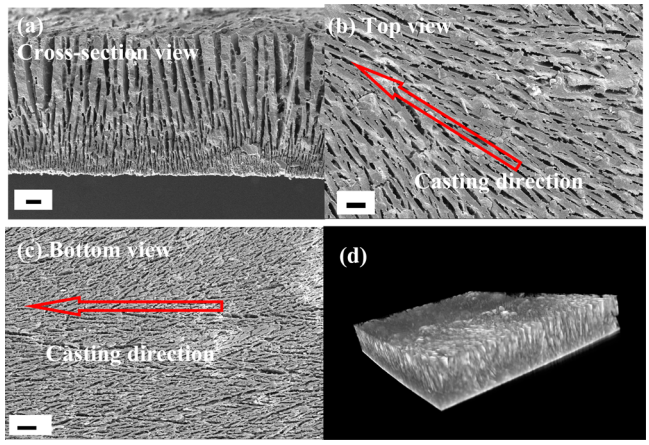

Figure 1. (a) Typical cross-section view of sintered substrate made through freeze-drying tape-casting; (b) surface view of the top part in panel a; (c) surface view of the bottom part in panel a (microbar = 100 μm); (d) 3D X-ray microscopy image of the anode substrate with dimensions of 3.03 × 3.72 × 0.55 mm.

Figure 1a shows the cross-section SEM view of the anode substrate, showing the characteristic graded open pores/channels, similar to previous reports.[16,21] The top part of the micrograph is the area away from the Myler polymer film, where the NiO−GDC tape is exposed to the environment, while the bottom part is the area close to the polymer film in the casting bed, on which ice nucleation started. Figure 1b,c shows the surface views of top part and bottom part in Figure 1a, respectively. Both top and bottom surface show an acicular morphology of ice crystals/pores, typical feature for freeze-

dx.doi.org/10.1021/am5003662 | ACS Appl. Mater. Interfaces 2014, 6, 5130−5136

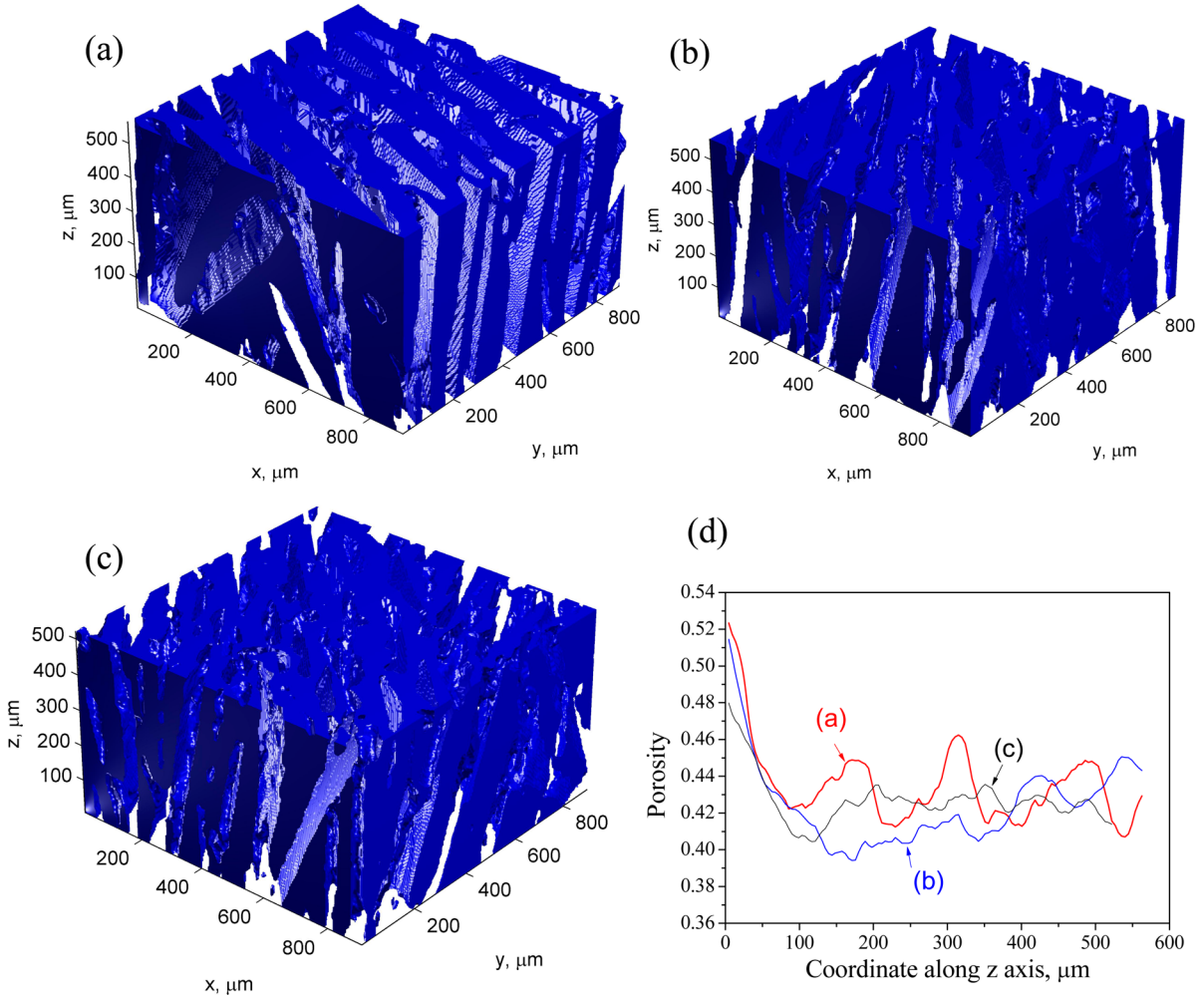

Figure 2. Reconstructed 3D microstructure images from the three different subdomains (a, b, and c) of porous NiO−GDC substrates. The blue/blank regions within the 3D images represent solid/pore phases. (d) Distribution of the local porosity along *z*-axis for the three different subdomains (a, b, and c).

drying tape-casting.[16] The pore/channel size (width) changes from about 10 μm on the bottom part to 20 μm on the top part of the NiO−GDC substrate shown in Figure 1a, indicating a gradient in size along the thickness direction. Figure 1d displays the 3D X-ray microscopic image of the anode substrate with dimensions of 3.03 × 3.72 × 0.55 mm. The bottom part in Figure 1d is the area close to the chilling Myler polymer film during the freeze tape-casting process, similar to that shown in Figure 1a.

To further study the NiO−GDC anode structure quantitatively, a 3D microstructure has been reconstructed by directly stacking the raw X-ray gray images along the *x*-axis in sequence. The interval step between images is 4.53 μm, the same as the resolution of the image. Figure 2a,b,c shows the reconstruction results for three different regions of the NiO−GDC substrate. To obtain the porosity distribution along the thickness direction (*z*-axis as shown in Figure 2a,b,c), two-dimensional (2D) slices are extracted from the segmented 3D matrix perpendicular to the *z*-axis, and then the 2D stereological method is employed.[22] Local porosity is caculated as the number fraction of pore pixels in the 2D slice. Figure 2d presents the porosity results, showing that local porosity is around 42% distributed along the thickness direction, similar to our previous results (49.01%) obtained from the mercury intrusion method.[15]

In general, the tortuosity factor of a conducting medium (solid phase for charge transport or pore phase for gas diffusion) is defined as[23]

$$\tau = \phi\sigma_0/\sigma_{\text{eff}} \quad (1)$$

where ϕ is the volume fraction of conducting medium, σ_0 is the conductivity or diffusivity of the pure conducting medium, and σ_{eff} is the effective conductivity or diffusivity of the porous conducting medium. σ_{eff} can be "measured" numerically by solving potential field within the conducting network. The potential obeys Laplace's equation:[24]

$$\Delta\psi = 0 \quad (2)$$

By enforcing a constant potential difference on the domain boundaries of *z*-axis, *y*-axis, or *x*-axis, the potential field distribution for a particular boundary condition is solved, and then the current or flux density through the network can be calculated. The conductivity or diffusivity ratio, $\sigma_0/\sigma_{\text{eff}}$ can then be obtained, which is independent of boundary conditions. Accordingly, the corresponding tortuosity factor in a particular direction can be calculated. A detailed description is published elsewhere.[18]

dx.doi.org/10.1021/am5003662 | ACS Appl. Mater. Interfaces 2014, 6, 5130−5136

In-house Matlab code has been developed to solve the Laplace's equation within a 3D network. Three 896 × 896 × 550 μm subdomains are extracted randomly from three different regions shown in Figure 2a,b,c followed by calculation, verifying that the domain size of 896 × 896 × 550 μm is sufficient to accurately calculate the tortuosity factor. Table 1 shows the calculation results of tortuosity factors for the three different subdomains. Along the thickness direction, a tortuosity factor of around 1.3 is obtained, which is much smaller than that for those sponge-like structured substrates (with a tortuosity factor value of 6−10).[25] From Table 1, it can also be seen that $\tau_z < \tau_x < \tau_y$ for the pore phases. The x-axis is the casting direction as shown in Figure 1. Although the NiO−GDC composite electrode is geometrically anisotropic, different region shows similar porosity or tortuosity factor along the thickness direction. The tortuosity factor in this study along the thickness direction is smaller than any other direction. It is expected that the gas diffusion resistance along the thickness direction will be substantially reduced during the fuel cell operations.

Table 1. Tortuosity Factors of Pore Phases along z-, y-, and x-Axises[a]

	pore phase		
sample No.	τ_z	τ_y	τ_x
1	1.270	39.182	2.359
2	1.328	7.464	4.767
3	1.235	16.587	3.640

[a]Three subdomains with a size of 896 × 896 × 550 μm are extracted randomly from the scanning regions for calculation.

Figure 3 shows the shrinkage of the NiO−GDC substrates made through either freeze-drying tape-casting or the conventional dry-pressing method with thin GDC film after sintering at different temperatures. Insets are SEM images of the surface of GDC film on freeze-drying tape-casted anode substrate. The shrinkage was calculated by measuring the diameter of substrates before and after high-temperature co-sintering. As shown in Figure 3, for the half cell sintered at 1450 °C for 12 h, the shrinkage of freeze-drying tape-casted substrate is about 19%, whereas the shrinkage of dry-pressed substrate is only 12%. Higher shrinkage of the anode substrate facilitates the densification of GDC film,[7] confirmed by the higher open circuit voltage. The more shrinked cell shows an OCV value of 0.88 V at 600 °C, much higher than that (0.79 V at 600 °C) for less shrinked cell under similar testing conditions. In addition, the porous surface of the green freeze-drying tape-casted substrate makes the connection between anode and electrolyte much better during drop-coating and co-sintering. In this study, for cell preparation, GDC film was prepared by co-firing GDC green film on the green freeze-drying tape-casted NiO−GDC substrates at 1450 °C for 12 h.

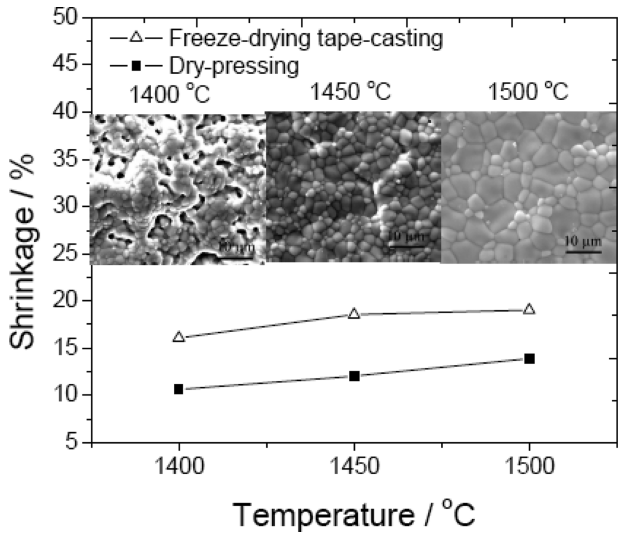

Figure 3. Shrinkage of GDC film on NiO−GDC sintered at different temperatures with NiO−GDC substrates made by either freeze-drying tape-casting or dry-pressing. Insets are surface views of GDC film on freeze-drying tape-casted substrate sintered at different temperatures.

Figure 4 shows the microstructure feature of the cell after electrochemical peformance measurement. The dense 30 μm thick GDC electrolyte film is well adhered to both the anode (~550 μm) and the cathode (~30 μm). As shown in Figure 4, the hierarchically oriented straight pores/channels are expected to facilitate mass transport in the anode.

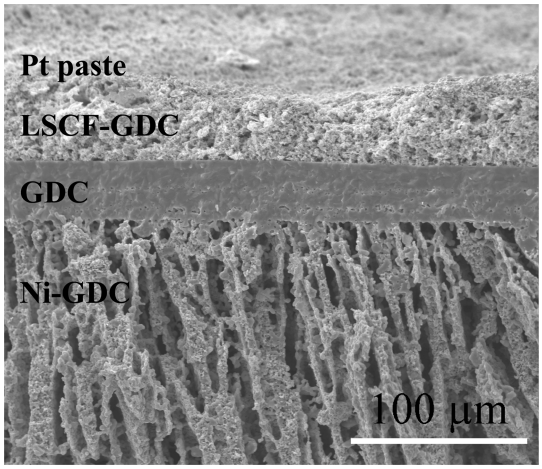

Figure 4. SEM images of cross sectional view of the cell after fuel cell testing.

Figure 5a shows the cell voltage, current, and power density curves of cells at different operating temperatures. The open circuit voltages (OCVs) of the cell are 0.929, 0.908, and 0.882 V at 500, 550, and 600 °C, respectively, which could be attributed to the minor electronic conduction of the GDC electrolyte due to the reduction of Ce^{4+} at the reducing atmosphere. But they are in good agreement with the values reported by others.[6,12] By contrast, at same conditions, the OCV values (for example, 0.79 V at 600 °C) for those through dry-pressing are lower, indicating that the freeze-drying tape-casted cell has a better electrolyte film.

As shown in Figure 5a, the maximum cell power densities (P_{max}) achieved are 0.292, 0.622, and 1.021 W cm^{-2} at 500, 550, and 600 °C, respectively, almost 2 times higher than the values for either the dry-pressed cell (at 600 °C, P_{max} for dry-pressed cell is only 0.489 W cm^{-2}) or other reported cell performance with similar cell materials and under similar testing conditions but with the traditional sponge-like microstructure of the anode.[6,26] The cell power output in this study using LSCF−GDC cathode is also comparable to the cell power output with $Ba_{0.5}Sr_{0.5}Co_{0.8}Fe_{0.2}O_3$ (BSCF) cathode,[27] which has been

dx.doi.org/10.1021/am5003662 | ACS Appl. Mater. Interfaces 2014, 6, 5130−5136

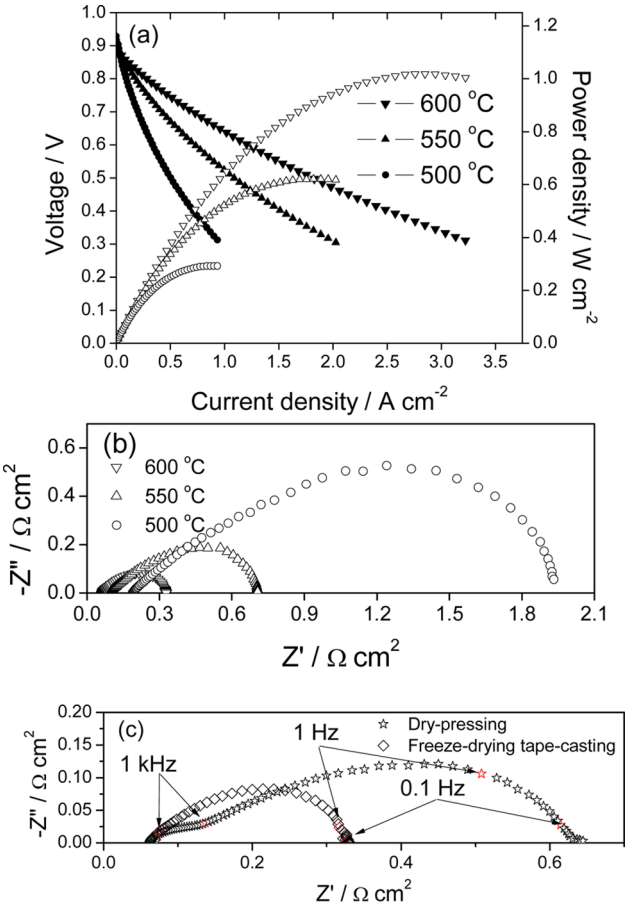

Figure 5. a IV and IP curves of cell measured at different operating temperature using hydrogen as fuel and ambient air as oxidant; b impedance spectra of cells tested at different temperature under open circuit conditions; (c) comparison of EIS for the cell with anode substrate through dry-pressing and freeze-drying tape-casting.

reported to have much higher catalytic activity than LSCF cathode, further demonstrating that high cell performance can be obtained by simply modifying the anode microstructure. Figure 5b shows the electrochemical impedance spectra of cells measured at different temperature under open circuit conditions. The ohmic resistance is 0.189, 0.096, and 0.061 Ω cm^2 at 500, 550, and 600 °C, respectively. The interfacial polarization resistance is 1.743, 0.6108, and 0.2672 Ω cm^2 at 500, 550, and 600 °C, respectively. Both the cell power density and interfacial polarization resistance obtained in this work are much better than those reported by others using similar cell materials but with cells fabricated from different processes (shown in Table 2). For example, a maximum power density of only 0.578 W cm^{-2} and an interfacial polarization resistance of 0.7 Ω cm^{-2} have been reported for SOFCs with a sponge-like porous Ni−GDC anode using the conventional uniaxial dry-pressing method, LSCF−GDC as cathode, and even much thinner GDC electrolyte film (10 μm).[26] For directly comparison, Ni−GDC anode supported cells with GDC film and LSCF−GDC cathode have also been prepared by dry-pressing, drop-coating and screen-printing. The composition and thickness for anode, electrolyte and cathode are kept same. The only difference is the anode microstructure. At 600 °C, the dry-pressed cells only show a peak power density of 0.489 W cm^{-2} and interfacial polarization resistance of 0.64 Ω cm^2 under same conditions.

Figure 5c shows the difference of impedance spectra for the cell prepared by dry-pressing and freeze-drying tape-casting. It is generally accepeted that the impedance in the high-frequency range corresponds to a combination of anode and cathode charge transfer processes,[28] while the impedance in the low-frequency range is associated with a gas diffusion process.[29] Because the electrolyte and cathode are kept the same for the cells made by freeze-drying tape-casting and dry-pressing, the difference in the two cell impedance spectra could be attributed to the anode. The comparison of these two cell spectra provides further evidence that both the activation and concentration polarization resistances have been decreased by applying a hierarchically oriented macroporous anode substrate made from the freeze-drying tape-casting process. The gas diffusion resistance through the anode can be estimated by the following equation:[30,31]

$$R_{\text{diffusion}_{(\text{anode})}} = \left(\frac{RT}{2F}\right)^2 l_a \frac{1}{D_{H_2O,H_2}} \frac{\tau_a}{\rho_a}\left(\frac{1}{p_{H_2}} + \frac{1}{p_{H_2O}}\right) \times \left(1.0133 \times 10^5 \frac{\text{Pa}}{\text{atm}}\right)^{-1} \quad (3)$$

where $R_{\text{diffusion}_{(\text{anode})}}$ is the gas diffusion resistance in the anode, R is the universal gas constant, T is the absolute temperature, F is the Faraday's constant, l_a is the anode thickness, D_{H_2O,H_2} is the binary diffusion coefficient for a mixture of H_2O and H_2, τ_a is the tortuosity factor of anode, and ρ_a is the volume fraction porosity of the anode, p_{H_2} and p_{H_2O} are the partial pressure of hydrogen and water vapor in the anode. Therefore, the gas diffusion resistance in anode could be decreased because the lower tortuosity and high porosity, similar as our previous report.[15]

The activation polarization loss from the anode can be written as[32]

Table 2. Comparison of Maximum Cell Power Desnity and Interfacial Polarization Resistance Measured at 600 °C of Anode Supported Cells Based on GDC or $Sm_{0.2}Ce_{0.8}O_2$ (SDC) Thin Film Electrolytes

cell configuration	P_{max}, W cm^{-2}	R_p, Ω cm^2	ref.
Ni−GDC/GDC(10 μm)/LSCF−GDC	0.578	~0.7	26
Ni−SDC/SDC(20 μm)/BSCF	1.01		27
Ni−GDC/GDC(16 μm)/LSCF	0.65		34
Ni−GDC/GDC(19 μm)/LSCF−GDC	0.39	0.50	35
Ni−GDC/GDC(3 μm)/LSCF	0.99		36
Ni−GDC/GDC(30 μm)LSCF−GDC	0.489	0.64	this study (dry-pressing)
Ni−GDC/GDC(30 μm)/LSCF−GDC	1.021	0.2675	this study (freeze-drying tape-casting)

dx.doi.org/10.1021/am5003662 | ACS Appl. Mater. Interfaces 2014, 6, 5130−5136

$$\eta_{act,anode} = \frac{2RT}{nF}\sinh^{-1}\left(\frac{i}{2i_0}\right) \quad (4)$$

where $\eta_{act,anode}$ is the activation loss from anode, n is the electron transferred per reaction, i is current density, and i_0 is the exchange current density. The exchange current density i_0 could be determined by the following equation:[33]

$$i_0 = nFc_R^* f_1 \exp\left(-\frac{\Delta G^*}{RT}\right) \quad (5)$$

where c_R^* is the reactant surface concentration, f_1 is the decay rate to products, ΔG^* is the activation barrier. The c_R^* may be described by

$$c_R^* = c_R - \frac{il_a}{nFD_{eff}} \quad (6)$$

where c_R is the flow channel reactant concentration, D_{eff} is the effective reactant diffusivity within catalyst layer. The effective diffusivity is normally determined by the porosity and tortuosity of the electrode (similar to eq 1) as the following equation:

$$D_{eff} = \frac{\rho_a}{\tau}D_0 \quad (7)$$

where D_0 is the diffusivity of fuel in pure pore phase. The tortuosity factor of pores for the hierarchically oriented NiO−GDC anode has been determined to be as low as 1.3 along the thickness direction, much smaller than that (typically 6−10) of the sponge-like porous anode,[25] consequently increasing the exchange current density and decreasing the anode activation polarization loss. Therefore, the hierarchically oriented pores in the Ni−GDC anode are expected to result in a lower resistance to mass transport of fuel (H_2) into and transport of reaction product (H_2O) away from the active area of the anode and increase the exchange current density in the anode/electrolyte interface, thus accelerating the reaction rate in the anode TPB area and enhancing the cell performance.

4. CONCLUSION

In summary, dense GDC film has been sucessfully fabricated on a hierarchically oriented NiO−GDC substrate by a simple and cost-effective combination of drop-coating and co-firing. The porosity distribution and tortuosity factor value along thickness direction have been determined both qualitatively and quantitatively from actual microstructure obtained nondestructively via 3D X-ray microscopy. This is new as, traditionally, such calculation could be only done based on either a 2D microstructure or an idealized 3D microstructure. The cells consisting of hierarchically oriented porous Ni−GDC anode, dense GDC thin film electrolyte and LSCF−GDC cathode show a high cell power output of 1.021 W cm^{-2} at 600 °C, which is almost 2 times higher than the values previously reported for cells with similar cell materials but with different Ni−GDC anode microstructure. Hierarchically oriented pores/channels in the anode lead to a low interfacial polarization resistance and consequently high cell power output. The method to fabricate a dense thin film on a hierarchically oriented porous substrate developed in this study can have broad applications in fuel cells and gas separation membranes.

AUTHOR INFORMATION

Corresponding Authors

*F. Chen. Tel: +1-803-777-4875. Fax: +1-803-777-0106. E-mail: chenfa@cec.sc.edu.

*M. Han. E-mail: hanminfang@sina.com.

Notes

The authors declare no competing financial interest.

ACKNOWLEDGMENTS

We're grateful to the financial support from National Science Foundation (1210792), the HeteroFoaM Center, an Energy Frontier Research Center funded by the U.S. Department of Energy, Office of Science, Office of Basic Energy Sciences under Award Number DE-SC0001061, the 973 Project (2012CB215404) and the NSFC (51261120378).

REFERENCES

(1) Singhal, S. C. Solid Oxide Fuel Cells for Stationary, Mobile, and Military Applications. *Solid State Ionics* **2002**, *152-153*, 405−410.

(2) Steele, B. C. H. Appraisal of $Ce_{1-y}Gd_yO_{2-y/2}$ Electrolytes for IT-SOFC Operation at 500 °C. *Solid State Ionics* **2000**, *129*, 95−110.

(3) Ding, D.; Li, X.; Lai, S. Y.; Gerdes, K.; Liu, M. Enhancing SOFC Cathode Performance by Surface Modification through Infiltration. *Energy Environ. Sci.* **2013**, *7*, 552−575.

(4) Cheng, M.-Y.; Hwang, D.-H.; Sheu, H.-S.; Hwang, B.-J. Formation of $Ce_{0.8}Sm_{0.2}O_{1.9}$ Nanoparticles by Urea-based Low-temperature Hydrothermal Process. *J. Power Sources* **2008**, *175*, 137−144.

(5) Tian, R.; Zhao, F.; Chen, F.; Xia, C. Sintering of Samarium-doped Ceria Powders Prepared by a Glycine-Nitrate Process. *Solid State Ionics* **2011**, *192*, 580−583.

(6) Ding, D.; Liu, B.; Zhu, Z.; Zhou, S.; Xia, C. High Reactive $Ce_{0.8}Sm_{0.2}O_{1.9}$ Powders via a Carbonate Co-Precipitation Method as Electrolytes for Low-Temperature Solid Oxide Fuel Cells. *Solid State Ionics* **2008**, *179*, 896−899.

(7) Yamaguchi, T.; Suzuki, T.; Shimizu, S.; Fujishiro, Y.; Awano, M. Examination of Wet Coating and Co-Sintering Technologies for Micro-SOFCs Fabrication. *J. Membr. Sci.* **2007**, *300*, 45−50.

(8) Chen, Y.; Bunch, J.; Jin, C.; Yang, C.; Chen, F. Performance Enhancement of Ni-YSZ Electrode by Impregnation of $Mo_{0.1}Ce_{0.9}O_{2+\delta}$. *J. Power Sources* **2012**, *204*, 40−45.

(9) Chen, Y.; Chen, F.; Ding, D.; Gao, J. Development and Fabrication of a New Concept Planar-Tubular Solid Oxide Fuel Cell (PT-SOFC). *Fuel Cells* **2011**, *11*, 451−458.

(10) Chen, Y.; Chen, F.; Wang, W.; Ding, D.; Gao, J. $Sm_{0.2}(Ce_{1-x}Ti_x)_{0.8}O_{1.9}$ Modified Ni−Yttria-Stabilized Zirconia Anode for Direct Methane Fuel Cell. *J. Power Sources* **2011**, *196*, 4987−4991.

(11) Sarikaya, A.; Petrovsky, V.; Dogan, F. Development of the Anode Pore Structure and Its Effects on the Performance of Solid Oxide Fuel Cells. *Int. J. Hydrogen Energy* **2013**, *38*, 10081−10091.

(12) Othman, M. H. D.; Droushiotis, N.; Wu, Z.; Kelsall, G.; Li, K. High-Performance, Anode-Supported, Microtubular SOFC Prepared from Single-Step-Fabricated, Dual-Layer Hollow Fibers. *Adv. Mater.* **2011**, *23*, 2480−2483.

(13) Cable, T. L.; Setlock, J. A.; Farmer, S. C.; Eckel, A. Regenerative Performance of the NASA Symmetrical Solid Oxide Fuel Cell Design. *J. Int. J. Appl. Ceram. Tec.* **2011**, *8*, 1−12.

(14) Gannon, P.; Sofie, S.; Deibert, M.; Smith, R.; Gorokhovsky, V. Thin Film YSZ Coatings on Functionally Graded Freeze Cast NiO/YSZ SOFC Anode Supports. *J. Appl. Electrochem.* **2009**, *39*, 497−502.

(15) Chen, Y.; Bunch, J.; Li, T.; Mao, Z.; Chen, F. Novel Functionally Graded Acicular Electrode for Solid Oxide Cells Fabricated by the Freeze-tape-casting Process. *J. Power Sources* **2012**, *213*, 93−99.

(16) Sofie, S. W. Fabrication of Functionally Graded and Aligned Porosity in Thin Ceramic Substrates with the Novel Freeze-tape-casting Process. *J. Am. Ceram. Soc.* **2007**, *90*, 2024−2031.

(17) Chen, Y.; Liu, Q.; Yang, Z.; Chen, F.; Han, M. High Performance Low Temperature Solid Oxide Fuel Cells with Novel Electrode Architecture. *RSC Adv.* **2012**, *2*, 12118−12121.
(18) Zhang, Y.; Xia, C.; Ni, M. Simulation of Sintering Kinetics and Microstructure Evolution of Composite Solid Oxide Fuel Cells Electrodes. *Int. J. Hydrogen Energy* **2012**, *37*, 3392−3402.
(19) Terwilliger, J. P.; Dizon, S. F. Salt Rejection Phenomena in the Freezing of Saline Solutions. *Chem. Eng. Sci.* **1970**, *25*, 1331−1349.
(20) Sofie, S. W.; Dogan, F. Freeze Casting of Aqueous Alumina Slurries with Glycerol. *J. Am. Ceram. Soc.* **2001**, *84*, 1459−1464.
(21) Wei, P.; Sofie, S.; Zhang, Q.; Petric, A. Metal Supported Solid Oxide Fuel Cell by Freeze Tape Casting. *ECS Trans.* **2011**, *35*, 379−383.
(22) Sahagian, D. L.; Proussevitch, A. A. 3D Particle Size Distributions from 2D Observations: Stereology for Natural Applications. *J. Volcanol. Geotherm. Res.* **1998**, *84*, 173−196.
(23) Iwai, H.; Shikazono, N.; Matsui, T.; Teshima, H.; Kishimoto, M.; Kishida, R.; Hayashi, D.; Matsuzaki, K.; Kanno, D.; Saito, M.; Muroyama, H.; Eguchi, K.; Kasagi, N.; Yoshida, H. Quantification of SOFC Anode Microstructure Based on Dual Beam FIB-SEM Technique. *J. Power Sources* **2010**, *195*, 955−961.
(24) Wilson, J. R.; Kobsiriphat, W.; Mendoza, R.; Chen, H.-Y.; Hiller, J. M.; Miller, D. J.; Thornton, K.; Voorhees, P. W.; Adler, S. B.; Barnett, S. A. Three-dimensional Reconstruction of a Solid-Oxide Fuel-Cell Anode. *Nat. Mater.* **2006**, *5*, 541−544.
(25) Cussler, E. L. *Diffusion: Mass Transfer in Fluid Systems*; Cambridge University Press: Cambridge, 1995.
(26) Leng, Y. J.; Chan, S. H.; Jiang, S. P.; Khor, K. A. Low-temperature SOFC with Thin Film GDC Electrolyte Prepared in situ by Solid-State Reaction. *Solid State Ionics* **2004**, *170*, 9−15.
(27) Shao, Z.; Haile, S. M. A High-Performance Cathode for the Next Generation of Solid-Oxide Fuel Cells. *Nature* **2004**, *431*, 170−173.
(28) Lai, W.; Haile, S. M. Impedance Spectroscopy as a Tool for Chemical and Electrochemical Analysis of Mixed Conductors: A Case Study of Ceria. *J. Am. Ceram. Soc.* **2005**, *88*, 2979−2997.
(29) Yoon, S. P.; Nam, S. W.; Han, J.; Lim, T.-H.; Hong, S.-A.; Hyun, S.-H. Effect of Electrode Microstructure on Gas-Phase Diffusion in Solid Oxide Fuel Cells. *Solid State Ionics* **2004**, *166*, 1−11.
(30) Virkar, A. V.; Chen, J.; Tanner, C. W.; Kim, J.-W. The Role of Electrode Microstructure on Activation and Concentration Polarizations in Solid Oxide Fuel Cells. *Solid State Ionics* **2000**, *131*, 189−198.
(31) Leonide, A.; Sonn, V.; Weber, A.; Ivers-Tiffée, E. Evaluation and Modeling of the Cell Resistance in Anode-Supported Solid Oxide Fuel Cells. *J. Electrochem. Soc.* **2008**, *155*, B36−B41.
(32) Chan, S. H.; Khor, K. A.; Xia, Z. T. A Complete Polarization Model of a Solid Oxide Fuel Cell and Its Sensitivity to the Change of Cell Component Thickness. *J. Power Sources* **2001**, *93*, 130−140.
(33) O'Hayre, R. P.; Cha, S.-W.; Colella, W.; Prinz, F. B. *Fuel Cell Fundamentals*; John Wiley & Sons: New York, 2006.
(34) Ding, C.; Lin, H.; Sato, K.; Amezawa, K.; Kawada, T.; Mizusaki, J.; Hashida, T. Effect of Thickness of $Gd_{0.1}Ce_{0.9}O_{1.95}$ Electrolyte Films on Electrical Performance of Anode-supported Solid Oxide Fuel Cells. *J. Power Sources* **2010**, *195*, 5487−5492.
(35) Zhen, Y. D.; Tok, A. I. Y.; Jiang, S. P.; Boey, F. Y. C. Fabrication and Performance of Gadolinia-Doped Ceria-Based Intermediate-Temperature Solid Oxide Fuel Cells. *J. Power Sources* **2008**, *178*, 69−74.
(36) Ding, C.; Hashida, T. High Performance Anode-Supported Solid Oxide Fuel Cell Based on Thin-Film Electrolyte and Nanostructured Cathode. *Energy Environ. Sci.* **2010**, *3*, 1729−1731.